




Construction and evaluation of liposomal drug delivery system for an ALK/HDACs dual-targeted inhibitor with sustained release and enhanced antitumor effect

Fang Ren¹ · Zongjie Gan¹ · Qianyu Zhang¹ · Dan He¹ · Baoyan Chen¹ · Xianwei Wu¹ · Xiaolin Zeng¹ · Kexin Wu¹ · Yangchen Xing¹ · Yan Zhang² · Huali Chen¹ 

Accepted: 3 June 2024
© Controlled Release Society 2024

Abstract

ALK/HDACs dual target inhibitor (PT-54) was a 2,4-pyrimidinediamine derivative synthesized based on the pharmacophore merged strategy that inhibits both anaplastic lymphoma kinase (ALK) and histone deacetylases (HDACs), which has demonstrated significant efficacy in treating multiple cancers. However, its poor solubility in water limited its clinical application. In this study, we prepared PT-54 liposomes (PT-54-LPs) by the membrane hydration method to overcome this defect. The encapsulation efficiency (EE) and particle size were used as evaluation indicators to explore the preparation conditions of PT-54-LPs. The morphology, particle size, EE, drug loading content (DLC), drug release properties, and stability of PT-54-LPs were further investigated. In vitro drug release studies showed that PT-54-LPs exhibited significant slow-release properties compared with free PT-54. PT-54-LPs also showed better tumor inhibitory effects than free PT-54 without significant adverse effects. These results suggested that PT-54-LPs displayed sustained drug release and significantly improved the tumor selectivity of PT-54. Thus, PT-54-LPs showed significant promise in enhancing anticancer efficiency.

Keywords 2,4-Pyrimidinediamine · Liposomes · Sustained-release · Antitumor efficacy

Abbreviations

ALK	anaplastic lymphoma kinase	DLS	dynamic light scattering
HDACs	histone deacetylases	TEM	transmission electron microscopy
PT-54	ALK/HDACs dual target inhibitor	PDI	polydispersity index
PT-54-LPs	liposomal formulation encapsulated PT-54	A549	human non-small cell lung cancer cell
Blank LPs	blank liposomes	HepG2	human hepatocellular carcinoma cells
DiR-LPs	DiR liposomes	4T1	mice breast cancer cells
EE	encapsulation efficiency	MDA-MB-231	human breast cancer cells
DLC	drug loading content	EPR	enhanced permeability and retention
		IC ₅₀	half maximal inhibitory concentration

✉ Huali Chen
chenhuali@cqmu.edu.cn

¹ Chongqing Key Laboratory of Biochemistry and Molecular Pharmacology, College of Pharmacy, Chongqing Medical University, Medical School Road, Yuzhong District, Chongqing 400042, PR China

² Yaopharma Co, Ltd, No. 100, Xingguang Ave, Chongqing 401121, China

Introduction

Cancer seriously threatens people's lives and health due to its high mortality rate. Currently, the primary clinical treatment methods for tumors are surgical excision, radiation, and chemotherapy [1]. Among them, chemotherapy remains one of the most frequently utilized therapies. Traditional cytotoxic chemotherapeutic drugs (including paclitaxel and platinum-based drugs) can be used to treat many cancers,

including breast cancer and lung cancer. However, because chemotherapeutic drugs lack selectivity for normal tissues and cells, they also have serious toxicity for normal tissues as well as organs while killing tumor cells, such as myelosuppression and severe negative impacts on the cardiovascular system [2, 3], which greatly restrict their clinical application. Therefore, developing novel anticancer medications is crucial to improving the therapeutic effects of cancer.

Anaplastic lymphoma kinase (ALK), a receptor-type protein tyrosine phosphokinase of the insulin receptor superfamily, is closely related to tumor development and has become a drug target for cancer treatment [4]. Histone deacetylases (HDACs) are enzymes that remove the acetyl group from histone lysine residues [5], which are essential for tumor cell proliferation, differentiation, and death. Therefore, developing inhibitors related to these targets is an effective strategy for treating cancer. PT-54 (Fig. 1), a 2,4-pyrimidinediamine derivative, was synthesized based on the pharmacophore merged strategy, which could inhibit both ALK and HDACs [6]. This type of multi-target molecular medicine was a new type of ALK/HDACs dual-target inhibitor that could solve the problem of tumor resistance to single-target drugs while avoiding issues caused by combination drugs such as drug-drug interactions. Preliminary studies showed that PT-54 inhibited the proliferation of many tumor cells (including HepG2, A549, MDA-MB-231, etc.) in vitro [6], demonstrating itself as a promising lead compound for inhibiting cancers such as liver, lung, and breast cancer. However, due to PT-54's poor water solubility, its clinical application was restricted. Therefore, it is necessary to develop a PT-54 formulation to address this defect of PT-54 and enhance its antitumor effects.

Over the past few decades, nano-drug delivery systems have provided several benefits to cancer therapeutic applications [7]. Due to the enhanced permeation and retention (EPR) effect, many nanoscale drug delivery systems have been utilized to prepare nanoscale antitumor drug

delivery systems with passive tumor-targeting features [8, 9]. Liposomes, as a nanodrug delivery technology, have shown considerable biocompatibility and biodegradability, which could improve the solubility of insoluble drugs in water and increase treatment effectiveness while decreasing toxicity [10]. Such as Lipusu®, a paclitaxel liposome-based injection, significantly improved its poor solubility in water, and enhanced the anti-tumor efficacy of paclitaxel while reducing the adverse effects of the drug [11, 12].

Despite the significant in vitro antitumor activity of PT-54, in vivo pharmacodynamic and systemic toxicity assessments have not been performed, and the solubility of PT-54 in water was extremely poor, therefore, the focus of this study was mainly on improving the solubility of PT-54 in water, as well as establishing animal tumor models to investigate the in vivo antitumor efficacy and safety of PT-54 and PT-54-LPs. Here, we established a liposome-based PT-54 delivery system (PT-54-LPs) in this research. As shown in Fig. 2, the PT-54-LPs were composed of soybean phosphatidylcholine and cholesterol, and the PT-54 was wrapped in a phospholipid bilayer, which substantially improved the defect of poor solubility of PT-54 in water. To extend the blood circulation duration and improve the stability in the blood circulation of PT-54-LPs, we used DSPE-mPEG2000. After screening the optimal formulation by orthogonal experiment, the characterization, in vitro drug release, stability, anti-tumor efficiency both in vivo and in vitro, as well as the safety of PT-54-LPs, were comprehensively evaluated. The results demonstrated that liposomes could improve the solubility of PT-54 in water and significantly reduce its systemic toxicity, and most importantly, although the PT-54-LPs did not exhibit stronger cytotoxic effects compared with free PT-54 in vitro, it showed stronger tumor inhibition and higher safety in vivo. These results demonstrated that PT-54-LPs were promising in cancer therapy.

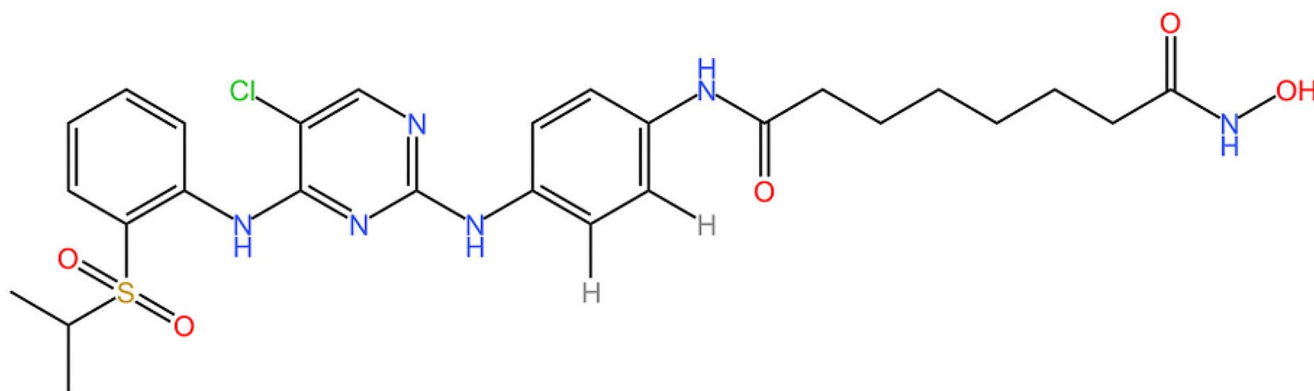


Fig. 1 Molecular structure of PT-54

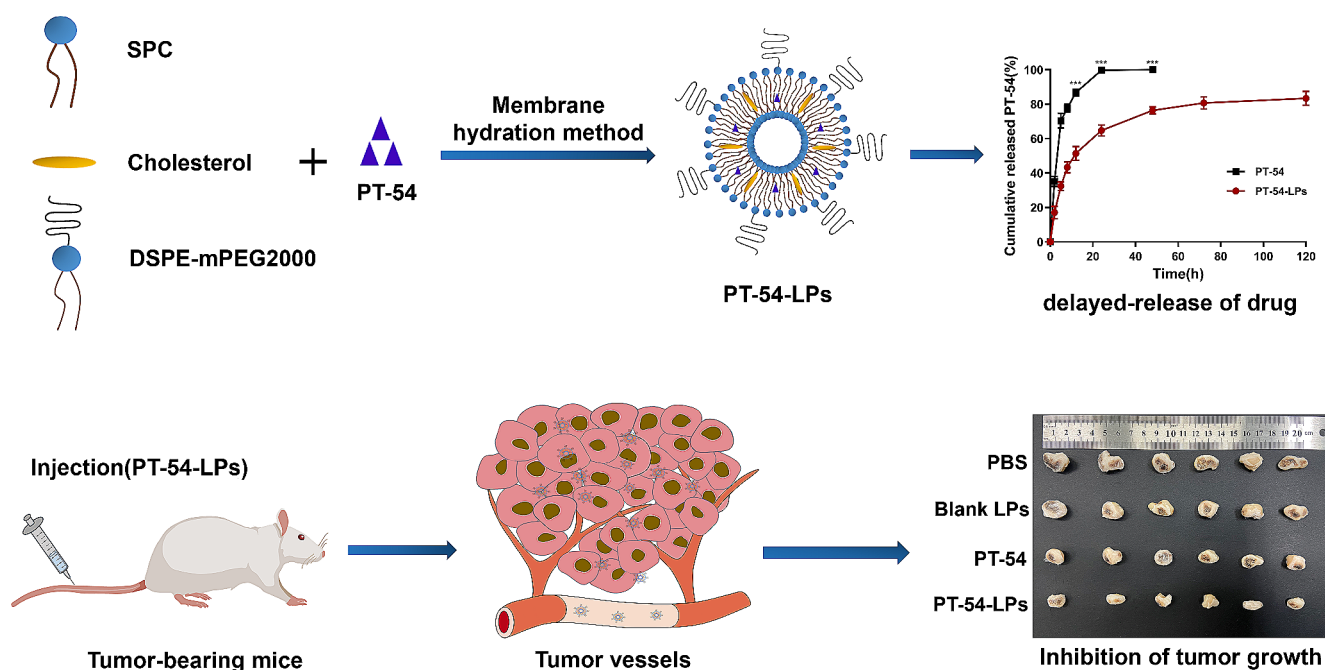


Fig. 2 The preparation of PT-54-LPs and tumor therapy

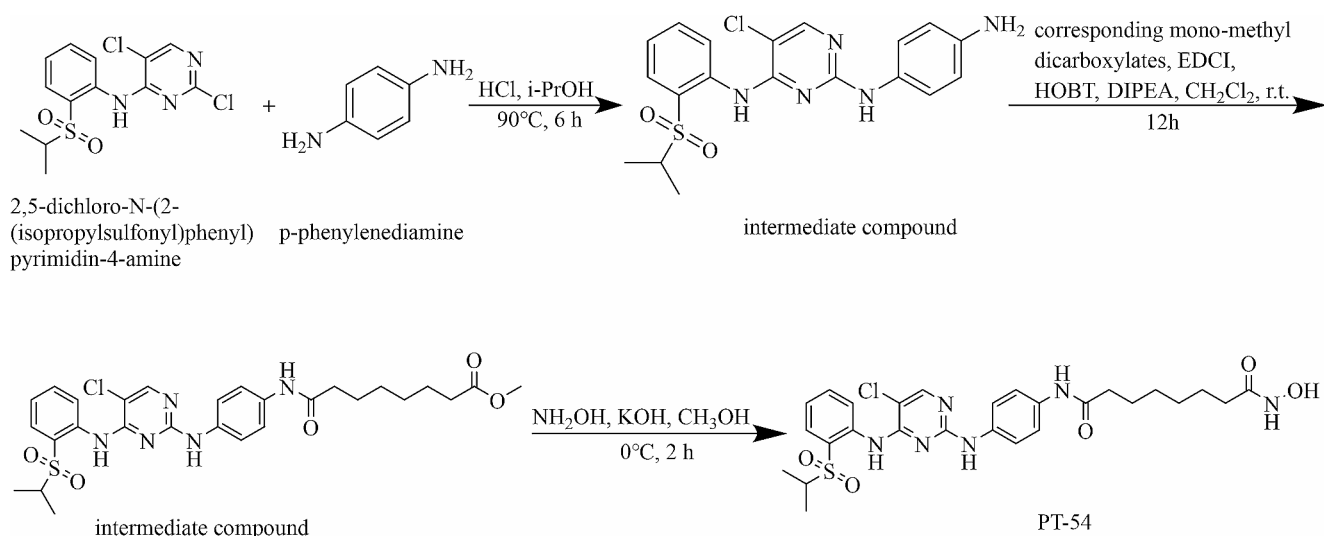


Fig. 3 The synthetic route of PT-54

Materials and methods

Materials

PT-54 (MW 589.2) was synthesized in our lab, and the synthetic route of the PT-54 compound is shown in Fig. 3. Soybean phosphatidylcholine (SPC), 1,2-distearoyl-sn-glycero-3-phosphoethanolamine-N [methoxy (polyethylene-glycol)-2000] (DSPE-mPEG2000), and cholesterol were obtained from Shanghai AVT Pharmaceutical Technology Co., Ltd (Shanghai, China). Sephadex G-50 (separation

range of 1,500–30,000) was purchased from Hefei Bomei Biotechnology Co., Ltd (Hefei, China). Fetal bovine serum (FBS) was obtained from Adamas Life, Shanghai Titan Technology Co., Ltd (Shanghai, China). Dulbecco's modified eagle medium (DMEM-high) and phosphate buffer solution (PBS) were obtained from Invitrogen (California, USA). Trypsin-EDTA solution, streptomycin/penicillin, and dialysis bags MD25 (Cut-off Mw: 8000–14,000 Da) were obtained by Beijing Solarbio Science & Technology Co., Ltd (Beijing, China). Cell counting kit-8 (CCK-8) was obtained from Big Biotech (Guangdong, China). DIR

IODIDE (DIIC18(7)) was purchased from Adamas Life, Shanghai Titan Technology Co., Ltd (Shanghai, China).

Cell lines

Mice breast cancer cells (4T1) and Human breast cancer cells (MDA-MB-231) were supplied by the Cell Bank of the Chinese Academy of Sciences (Shanghai, China). Two kinds of cells were cultured in DMEM high glucose medium containing 10% fetal bovine serum (FBS) and 1% penicillin and streptomycin. The cells were cultivated at 37 °C in moist air with 5% CO₂ in a cell culture incubator.

Animals

Female BALB/c mice (20 g body weight) were provided by the Experimental Animal Centre of Chongqing Medical University (Chongqing, China). Fed animals standardized food and allowed them to drink freely. All animal operations followed the Chongqing Management Approach to Laboratory Animals (Chongqing government order NO.195).

Preparation of PT-54-LPs

PT-54-LPs were prepared by the membrane hydration method [13], and the optimal formulation was obtained by the L₉ (3³) orthogonal experiment. In short, the membranes were dissolved in chloroform, and PT-54 was dissolved in a solvent mixture of dichloromethane and methanol (1:1, v/v). Membranes and PT-54 were added to a rotary evaporation flask, and the lipid films were formed by rotary evaporation using a rotary evaporator at 37 °C and 90~120 rpm under a reduced pressure vacuum until no organic solvent remained. Phosphate buffer (PBS, pH=7.4) was then added, and the films were allowed to fully hydrate in a shaker at 37 °C at 150 rpm. The probe-type ultrasonicator was applied to disperse the lipid film uniformly at 250 W, and unencapsulated PT-54 was removed by Sephadex G-50 [14]. The final PT-54-LPs were collected and kept at 4 °C for further analysis. In some studies, DiR was loaded in liposomes (DiR-LPs) in place of PT-54 to track the biodistribution of liposomes in vivo, and the ultimate DiR dosage was 20 µg/mL.

Characterization of PT-54-LPs

The morphologies of PT-54-LPs were observed by TEM (Jeol, JEM-2100, Japan). PT-54-LPs were prepared as described above, diluted 5-fold with PBS buffer at room temperature, and then dropped on a copper grid. After 10 min of incubation, the sample was stained with 2% (w/v) aqueous phosphotungstic acid. The copper mesh was air-dried and observed by TEM at room temperature.

A dynamic light scattering analyzer (DLS, Malvern, ZEN3600, United Kingdom) was used to assess the size distribution, PDI, and zeta potential of PT-54-LPs. The sample solution was diluted 20-fold using PBS buffer. The measurement temperature was 25 °C and the samples were measured in triplicate. To assess PT-54-LPs encapsulation efficiency (EE) and drug loading content (DLC), Sephadex G-50 microcolumn centrifugation was used to separate free PT-54 from PT-54-LPs. Briefly, overnight-soaked Sephadex G-50 was filled into a 5 mL syringe and the centrifuged solution was collected by centrifugation at 1,500 r/min for 2 min. The absorbance of PT-54 was measured by the ultraviolet-visible spectrophotometry method at 289 nm. The concentration of the drug encapsulated in PT-54-LPs was calculated as C₁, and the total concentration of the drug was determined as C₀ from the liposome mixture without passing through the column. The EE and DLC were obtained using the following formula:

$$EE (\%) = C_1 / C_0 \times 100\%$$

$$DLC (\%) = M_1 / M_2 \times 100\%$$

where M₁ was the amount of PT-54 in the liposome and M₂ represented the total PT-54 plus the amount of membrane material.

Solubility assessment of PT-54-LPs

Excess PT-54 powder and lyophilized PT-54-LPs were dispersed in 5 mL of ultrapure water for solubility determination, respectively, and shaken in a shaker at 37 °C, 100 rpm for 48 h. After 48 h, the samples were taken out, left at room temperature for 24 h, and then centrifuged at 4,000 rpm for 10 min. The content of PT-54 in the supernatant was determined by the ultraviolet-visible spectrophotometry method.

The low-temperature storage stability and in vitro serum stability studies

To evaluate the storage stability of liposomes, PT-54-LPs were stored in a 4 °C fridge for 14 days, and the size distribution, PDI, zeta potential, EE, DLC, and leakage rate of the PT-54-LPs were measured. To investigate the stability of PT-54-LPs in serum, the prepared PT-54-LPs were measured by co-incubation with PBS and 10% FBS for 3 days, respectively, and the size distribution, PDI, zeta potential, and EE of PT-54-LPs were monitored every day. The leakage rate was calculated by the following formula:

$$Leakage\ rate = (1 - E_n / E_0) \times 100\%$$

where E_n was the encapsulation efficiency at different storage time points, and E_0 was the initial drug encapsulation efficiency.

Hemolysis assay

Blood was taken from the sockets of female BALB/c mice and collected in centrifuge tubes containing sodium heparin, washed three times with saline to remove fibrinogen, and a 2% (w/v) RBC suspension was then made by dilution with saline. Then PT-54-LPs were mixed with a 2% (w/v) suspension of red blood cells, the saline was used as a negative control and 1% Triton 100x as a positive control and incubated at 37 °C for 3 h. After incubation, centrifugation was performed at 1500 rpm for 15 min. The supernatant (100 μL) was taken and the absorbance value was detected at 545 nm using an automatic microplate reader (LabServ®, Thermo Fisher Scientific). The hemolysis rate (HR%) was calculated according to the following formula:

$$HR\% = \frac{(A_{test\ group} - A_{negative})}{(A_{positive} - A_{negative})} \times 100\%$$

In vitro PT-54 release from LPs

1 mL of PT-54-LPs or PT-54 solution was sealed in dialysis bags (MWCO = 8–14 kDa), and then the dialysis bags were incubated in 30 mL of PBS buffer at pH 7.4. Besides, 2% SDS and 20% anhydrous ethanol were added to the release medium to facilitate the drug release process [14, 15]. The dialysis bags were then kept in a shaking incubator at 37 °C with a rotating speed of 100 rpm. After 2, 5, 8, 12, 24, 48, 72, and 120 h, 1 mL of the release medium was taken out and replaced with a new release medium of the same volume. Finally, concentrations of PT-54 were measured by the ultraviolet-visible spectrophotometry method at a wavelength of 289 nm and their release profiles were plotted.

In vitro cytotoxicity assays

Cell Counting Kit-8 (CCK-8) was used to assess the cytotoxicity of PT-54-LPs in vitro. 4T1 cells and MDA-MB-231 cells were seeded into 96-well plates at a density of 4000 cells per well, respectively, and then incubated at 37 °C in an incubator with 5% CO₂ for 24 h. The cells were then treated with various drug formulations (Blank-LPs, free PT-54, and PT-54-LPs) for 24 and 48 h, respectively. In this process, free PT-54 was dissolved in DMSO solvent and diluted with culture medium to the specified concentration, in which the amount of DMSO did not exceed 1% and had no effect on cell viability. After 24 and 48 h, the medium was altered

with a solution comprising 90 μL fresh medium and 10 μL CCK-8, and the incubation continued for 1 h at 37 °C. The solution absorbance was measured by a microplate reader (LabServ®, Thermo Fisher Scientific) at 450 nm, and cell viability was determined using the following equation:

$$Cell\ viability(\%) = \frac{(OD_{experiment} - OD_{blank})}{(OD_{control} - OD_{blank})} \times 100\%$$

In vivo imaging and anti-tumor assessment

To establish animal tumor models, female BALB/c mice (20 g body weight) were injected subcutaneously with 1×10^6 4T1 cells in the right forelimb. A near-infrared (NIR) small animal imaging system was utilized to assess the bio-distribution of liposomes in vivo as the tumor size reached 100–150 mm³. Mice were anesthetized by intraperitoneal injection of 1% pentobarbital sodium. Considering PT-54 lacks fluorophores, DiR was used to replace it to investigate in vivo fluorescence imaging of liposomes. DiR-LPs were injected into the tail vein of mice, and the tumoral retention of liposomes was measured at 2, 4, 10, 24, 48, 72, 96, and 120 h. At 48 h, the mice were executed, and their main organs (hearts, livers, spleens, lungs, and kidneys) and tumors were collected for fluorescent analysis.

To assess the anticancer efficiency of the PT-54-LPs in vivo, the 4T1 tumor-bearing BALB/c female mice were randomly divided into four groups: (1) PBS, (2) Blank-LPs, (3) free PT-54 (dissolved in PBS solution containing 10% DMSO and 1% Tween 80), and (4) PT-54-LPs. Then the formulations were administered (300 μL in volume, with a dose equivalent to PT-54 15 mg/kg) every other day for 4 times, respectively. Tumor volumes and weight changes in all groups were measured every other day to assess the therapeutic efficacy of the drugs. Tumor volume was determined as (tumor's longest diameter × (tumor's shortest diameter)²)/2. On day 13, mice were killed, and tumors were collected, photographed, and weighed. Meanwhile, the tumor inhibition rates of drugs were calculated by the following equation: (1 - tumor weight in the experimental group/tumor weight of the control group) × 100%.

To evaluate the systemic toxicity of PT-54-LPs, female BALB/c mice (20 g body weight) were stochastically divided into four groups and intravenously injected with PBS, Blank-LPs, free PT-54, and PT-54-LPs (300 μL, PT-54-equivalent dose of 15 mg/kg) every other day for 4 times, respectively. On day 13, the mice were killed, and blood samples were taken from their sockets for blood routine and biochemical analysis. The evaluation indicators include liver functions (ALP, alkaline phosphatase; AST, aspartate aminotransferase; ALT, alanine aminotransferase), renal

Table 1 Factors and Levels in Orthogonal Design

Level	Factor		
	A	B	C
1	4:1	1:20	1:20
2	6:1	1:30	1:30
3	8:1	1:40	1:40

Note: A: ratio of SPC to cholesterol (n/n); B: ratio of DSPE-mPEG2000 to SPC (n/n); C: ratio of PT-54 to SPC (n/n)

functions (CREA, creatinine; UREA, urea; UA, uric acid), and hematological functions (WBC, white blood cells; PLT, platelet).

After in vivo anticancer studies, their main organs and tumors were collected, fixed in 4% paraformaldehyde, and embedded in paraffin. Slices approximately 5- μ m thick were made from paraffin-embedded tissues for histological analysis, and hematoxylin and eosin (H&E) were used to assess tissue staining according to a light microscope [16].

Statistical analysis

All data were provided as the mean \pm standard deviation. GraphPad Prism 9.0 software was applied for statistical analysis. $P < 0.05$ indicated statistical significance.

Results and discussion

Preparation of PT-54-LPs

The formulation of PT-54-LPs was optimized by $L_9(3^3)$ orthogonal experiments, and the drug encapsulation efficiency (EE) was used as an evaluation index to explore the

optimal formulation of PT-54-LPs. As shown in Table 1, we selected three factors that had a major impact on the EE of PT-54-LPs and designed orthogonal experiments to find the optimal formulation process conditions: (A) the ratio of SPC to cholesterol (n/n), (B) the ratio of DSPE-mPEG2000 to SPC (n/n), and (C) the ratio of PT-54 to SPC (n/n). As shown in Table 2, the EE of PT-54-LPs was within a range of 48–73%, and the impact of the ranking of the factors on EE was $C > B > A$. The optimal formulation was $A_2B_1C_2$, with the ratios of SPC to cholesterol, DSPE-mPEG2000 to SPC, and PT-54 to SPC at 6:1, 1:20, 1:30, respectively. In the optimal formulation, PT-54-LPs had an encapsulation efficiency (EE) of 73% and a drug loading content (DLC) of 1.5%.

Characterization of PT-54-LPs

We used the membrane hydration method to prepare and characterize liposomes with the optimal formulation. As shown in Fig. 4A, we obtained liposomes with light blue opalescence. PT-54-LPs had a particle size of around 101.12 ± 1.62 nm, indicating that they are single-compartment liposomes, and the PDI was approximately 0.21 ± 0.02 . The EPR effect has been shown to lead to effective tumoral accumulation of liposomes with particle sizes in the range of 100 to 200 nm [17, 18]. The EPR effect of solid tumors greatly helped the selective distribution of lipid-based drugs in tumors, which could increase efficacy and reduce systemic adverse effects of drugs [19, 20]. Therefore, PT-54-LPs could efficiently concentrate at the tumor site by utilizing this feature, resulting in better therapeutic effects. Images of transmission electron microscopy (TEM) showed

Table 2 Orthogonal experimental design and results

NO.	A	B	C	D	EE%
1	1	1	1	1	56.2
2	1	2	2	2	71.43
3	1	3	3	3	67.69
4	2	1	2	3	73.05
5	2	2	3	1	62.87
6	2	3	1	2	48.1
7	3	1	3	2	69.81
8	3	2	1	3	57.72
9	3	3	2	1	58.81
K_1	195.32	199.06	162.02	177.88	
K_2	184.02	192.02	203.29	189.34	
K_3	186.34	174.6	200.37	198.46	
k_1	65.11	66.35	54.01	59.29	
k_2	61.34	64.01	67.76	63.11	
k_3	62.11	58.20	66.79	66.15	
R	3.77	8.15	12.78	6.86	
Major-minor order	$C > B > A$				
Optimal parameter	A_2	B_1	C_2		
Optimal combination	$A_2B_1C_2$				

Note: A: ratio of SPC to cholesterol (n/n); B: ratio of DSPE-mPEG2000 to SPC (n/n); C: ratio of PT-54 to SPC (n/n); D: error phase. K_1 , K_2 , and K_3 represent the sum of indicators at each level of each factor; k_1 , k_2 , and k_3 represent the average scores of indicators at each level of each factor; R represents the mean score range of each factor ($R = k_{\max} - k_{\min}$)

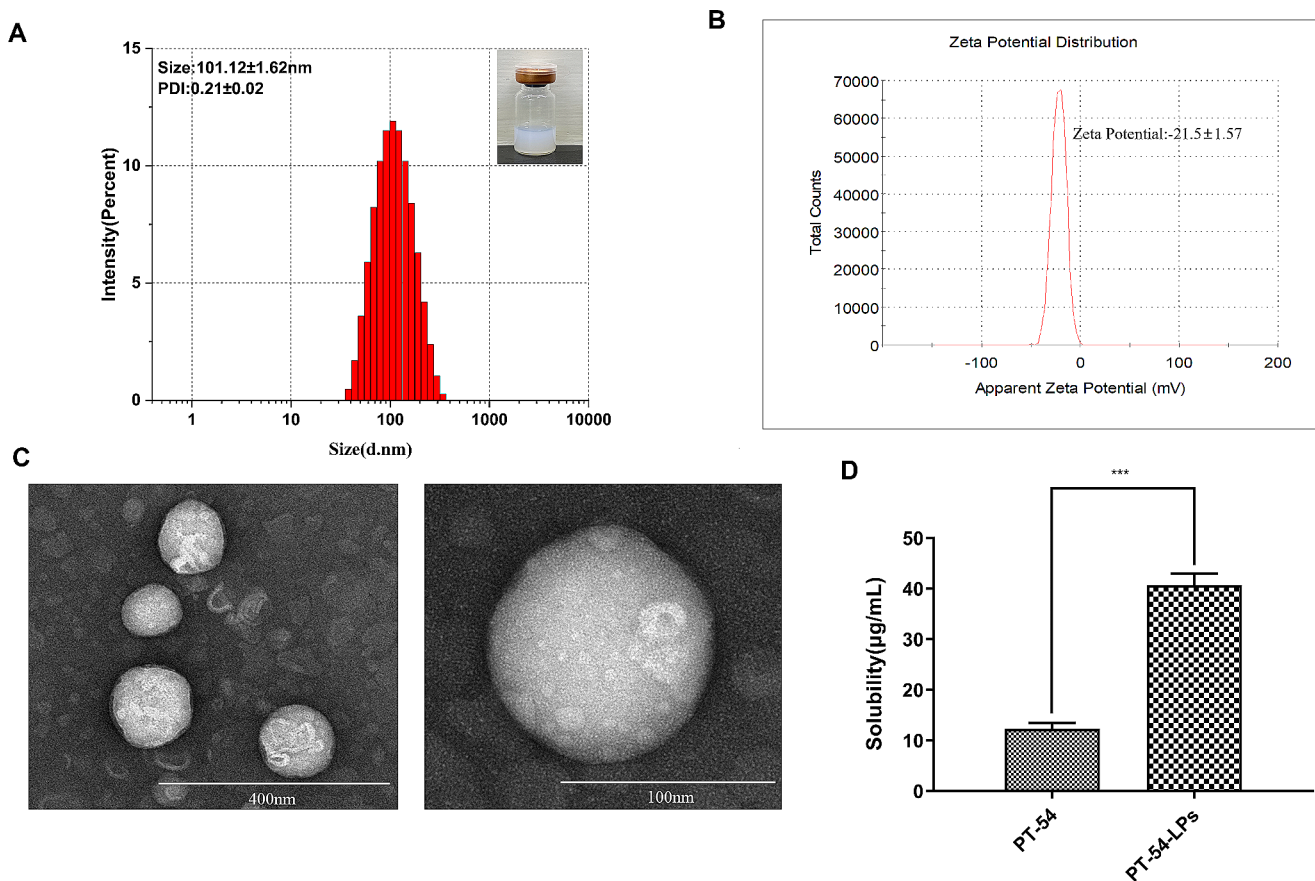


Fig. 4 Characterization of PT-54-LPs. (A) Particle size and PDI. (B) Zeta potential. (C) TEM images. (D) Solubility of PT-54 and PT-54-LPs in water. Data were represented as mean \pm SD ($n=3$), where ***: $p < 0.001$, compared with the PT-54-LPs

(Fig. 4C) that PT-54-LPs had a spherical shape, and the particle size was around 100 nm; the result matched DLS results (Fig. 4A). The zeta potential of PT-54-LPs was around -21.5 ± 1.57 mV (Fig. 4B). It has been reported that the negative electrical properties of the liposome surface can maintain the stability of liposome formulations through electrostatic repulsion [21]. The potential of PT-54-LPs was -21.5 ± 1.57 mV, which contributes to the physical stability of PT-54-LPs during the storage period.

In addition, we investigated the solubility of PT-54 and PT-54-LPs separately in water (Fig. 4D), and the results showed that the solubility of PT-54 and PT-54-LPs in water were 12.33 ± 1.19 $\mu\text{g/mL}$ and 40.69 ± 2.28 $\mu\text{g/mL}$ ($P < 0.001$), respectively. The result showed that preparing PT-54 into liposomes significantly improved its solubility in water.

The low-temperature storage stability and in vitro serum stability studies

Low-temperature storage was often applied in short-term liposome drug preservation [22]. Therefore, we investigated the low-temperature storage stability of PT-54-LPs.

The EE, DLC, particle size, zeta potential, PDI, and leakage rate of PT-54-LPs did not significantly change within 14 days in low-temperature storage (4°C). The results are shown in Fig. 5A-C. All the indexes of PT-54 liposomes did not change significantly in 14 days, and the leakage rate of PT-54-LPs was 6.7%, which was below 10%, these results indicated that PT-54 liposomes have good stability under the storage condition of 4°C .

The stability of liposomes during in vivo circulation can be simulated by serum stability tests [23]. Therefore, we evaluated the stability of liposomes in 10% fetal bovine serum and PBS, respectively [24, 25]. The size, zeta potential, PDI, and EE of PT-54-LPs exhibited good stability in these two media within three days (Fig. 6A-D). These results indicated that PT-54-LPs had good serum stability and were suitable for intravenous administration. This might be due to the PEG hydrophilic layer that could protect the surface charge of liposomes, reduce interaction with plasma proteins, and increase liposome stability.

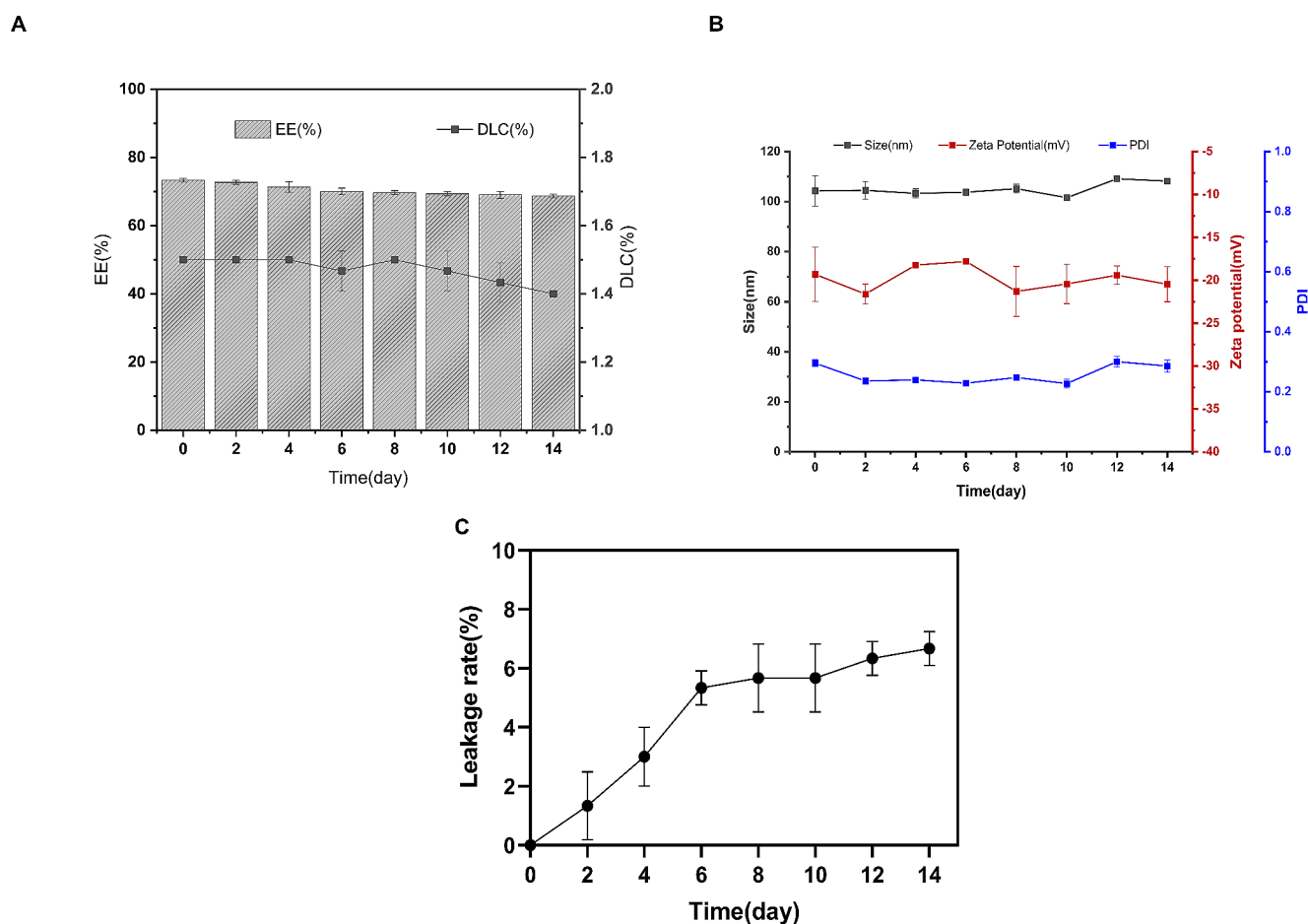


Fig. 5 The low-temperature storage stability. (A) encapsulation efficiency (EE) and drug loading content (DLC) of PT-54-LPs stored at 4 °. (B) Size, PDI, and zeta potential of PT-54-LPs stored at 4 °. (C) Leakage rate of PT-54-LPs at 4 °C. Data represented as mean \pm SD ($n = 3$)

Hemocompatibility of PT-54-LPs

In vitro hemolysis assays could evaluate the biosafety of intravenously injected drugs [26]. Therefore, we investigated the in vitro hemolytic activity of PT-54-LPs. As shown by the results of the hemolysis rate (Fig. 7), the hemolysis rate in the PT-54-LPs group was 0.16% when the drug concentration was 1 mg/mL, which indicated that PT-54-LPs had good blood compatibility and were suitable for intravenous injection.

In vitro release behavior

The release profiles of the PT-54 solution and PT-54-LPs were displayed in Fig. 8. The cumulative release of the PT-54 solution reached 87% within 12 h and was completely released within 24 h. However, PT-54-LPs released only 51% of PT-54 at 12 h and 65% at 24 h, with a cumulative release of 83% at 120 h, indicating that PT-54-LPs showed significant sustained release behavior. The capability of releasing drugs in a sustained manner was an important characteristic of liposomes [27], as the drugs were encapsulated by a stable

lipid bilayer, and the diffusing or dissolving of the liposome skeleton led to the slow release of the drug [28, 29].

In vitro cytotoxicity

The Cell Counting Kit-8 (CCK-8) was used to evaluate the cytotoxicity [30] of Blank LPs, PT-54-LPs, and free PT-54 against 4T1 and MDA-MB-231 cells in vitro. Blank LPs and PT-54-LPs were prepared using the same prescription and process parameters. In cytotoxicity assessment, blank liposomes and PT-54 liposomes were administered to the cells using the same dilutions, and ultimately, the lipid concentration of the blank liposomes was the same as that of the drug-carrying liposomes. As shown in Fig. 9A-D, after being treated with Blank-LPs, the vitality of both cells was greater than 90%. This result demonstrated that blank liposomes had no obvious cytotoxicity and could be utilized as a safe carrier for drug delivery. Dose-dependent cell toxicity was observed in both cells after 24 and 48 h of treatment with PT-54-LPs and free PT-54, respectively. Notably, free PT-54 showed a more significant inhibitory effect on cancer cells compared with the PT-54-LPs

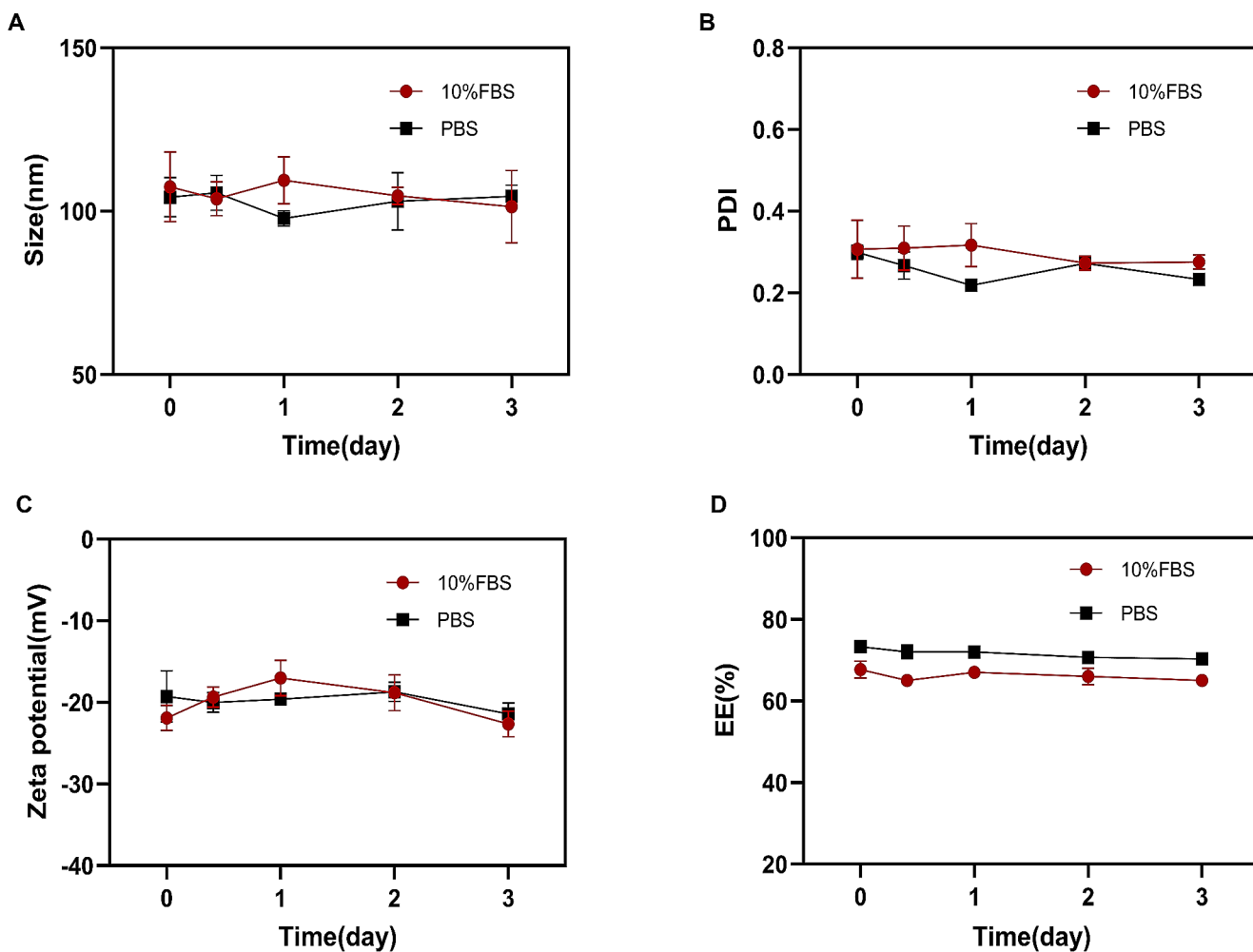


Fig. 6 Stability of PT-54-LPs in 10% FBS and PBS for 72 h. (A) Size changes of PT-54-LPs. (B) PDI changes of PT-54-LPs. (C) Zeta potential changes of PT-54-LPs. (D) EE changes of PT-54-LPs. Data represented as mean \pm SD ($n=3$)

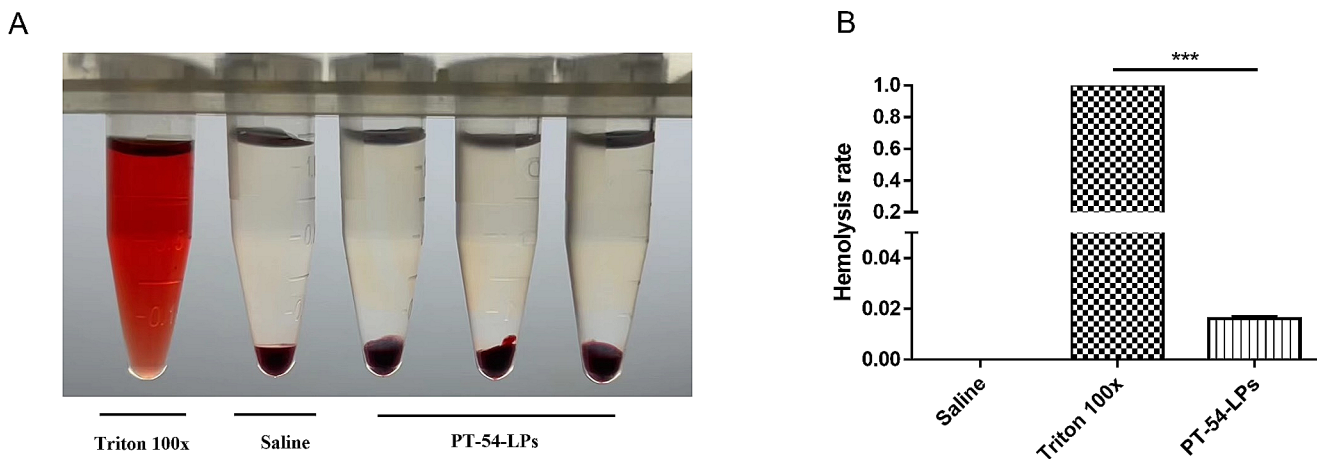


Fig. 7 Hemolysis results of PT-54-LPs, (A) Hemolysis images of PT-54-LPs, (B) Hemolysis rate of PT-54-LPs. Data were represented as mean \pm SD ($n=3$), where ***: $p < 0.001$, compared with the Triton 100x

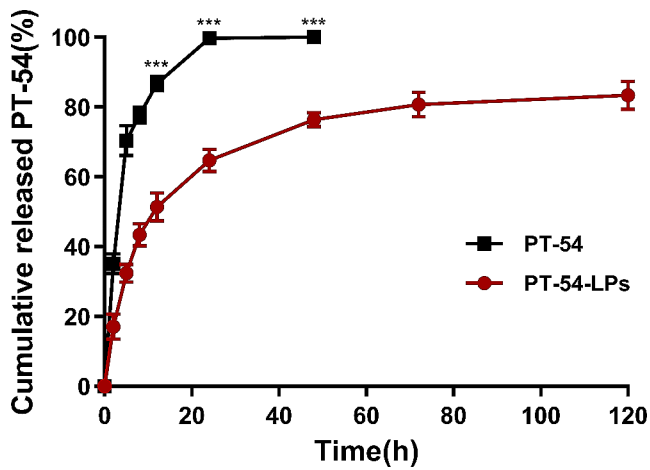


Fig. 8 In vitro release of PT-54 solution and PT-54-LPs at pH 7.4. Data represented as mean \pm SD ($n=3$), where ***: $p < 0.001$, compared with the PT-54-LPs

Table 3 IC_{50} of PT-54 and PT-54-LPs

IC_{50} ($\mu\text{g/mL}$)	4T1		MDA-MB-231	
	24 h	48 h	24 h	48 h
PT-54	1.13	0.11	1.67	0.26
PT-54-LPs	7.32	0.40	9.14	1.02

group at both 24 h and 48 h under the same doses. When the drug concentration reached 10 $\mu\text{g/mL}$, the cell viability of 4T1 and MDA-MB-231 in the free PT-54 group was only 17% and 18% at 24 h, respectively, and there were almost no cells survived in the free PT-54 group at 48 h. However, the survival of 4T1 and MDA-MB-231 cells treated with the same concentration of PT-54-LPs were 41% and 48% at 24 h, 17% and 24% at 48 h, respectively. As shown in Table 3, the IC_{50} values of free PT-54 were significantly lower compared with PT-54-LPs. The result could be explained by the results from the in vitro release study as indicated in 3.4 (Fig. 8). Free PT-54

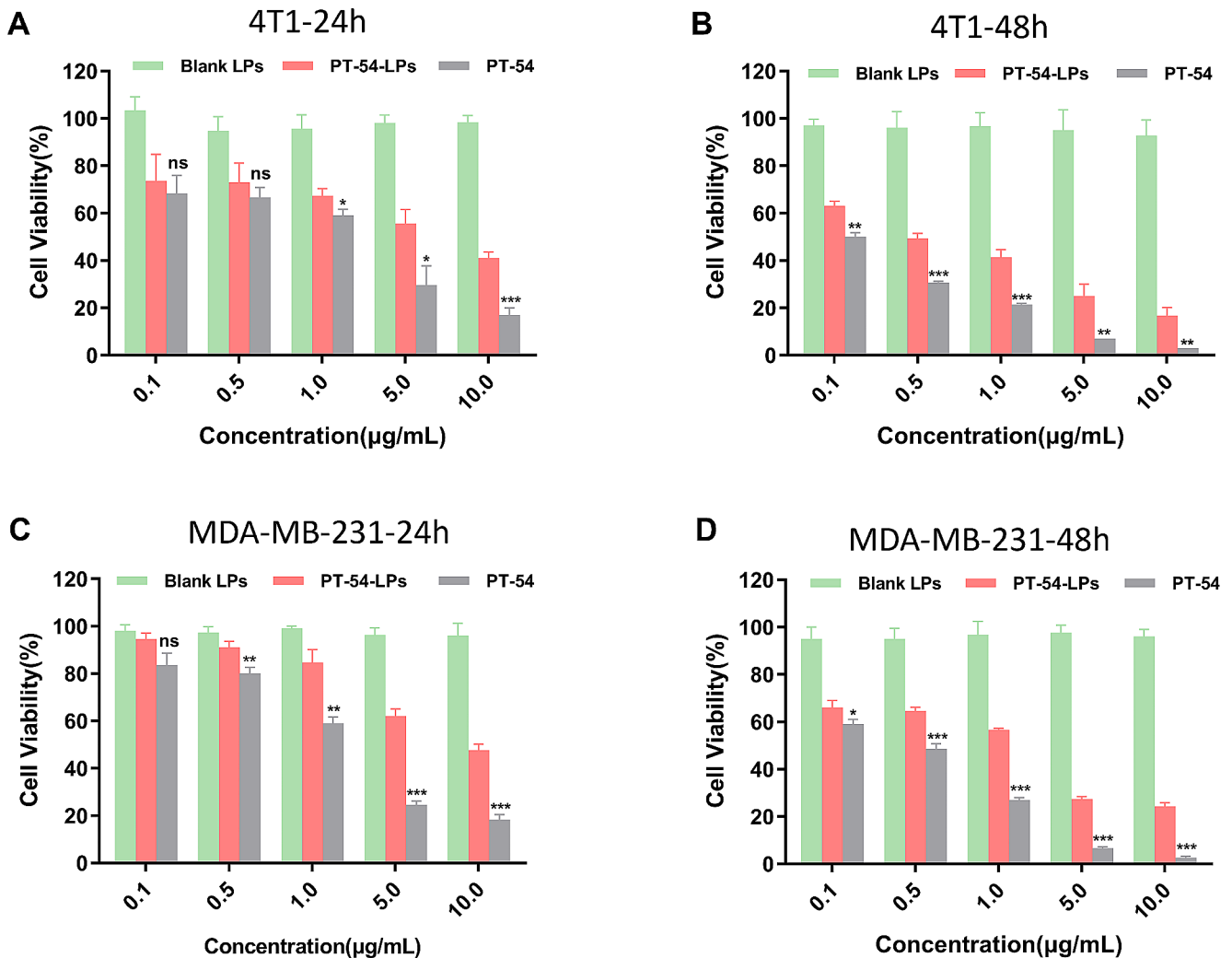


Fig. 9 The inhibitory effects of blank liposomes, PT-54-LPs, and PT-54 on cell proliferation of 4T1 and MDA-MB-231. (A) Inhibition effect on 4T1 cells (24 h); (B) Inhibition effect on 4T1 cells (48 h); (C) Inhibition effect on MDA-MB-231 cells (24 h); (D) Inhibition effect

on MDA-MB-231 cells (48 h). Data represented as mean \pm SD ($n=3$), where ns: $p > 0.05$, *: $p < 0.05$, **: $p < 0.01$, ***: $p < 0.001$, compared with the PT-54-LPs group

was almost completely released after 24 h, while only 65% of PT-54 was released from PT-54-LPs within 24 h and 76% after 48 h. It has been shown that anticancer efficacy *in vitro* was closely related to the free drug accessible in tumor cells [31]. Therefore, the stronger inhibitory effect of free PT-54 on cancer cells might be attributed to the fact that PT-54 could enter tumor cells quickly by diffusion, while in the PT-54-LPs group, the drug was encapsulated into liposomes released in a relatively slow fashion, which led to the lower inhibitory effect of PT-54-LPs on cancer cells than free PT-54.

Tumor accumulation of PT-54-LPs

To investigate the tumor targeting and retention of liposomes, DiR was loaded into liposomes as a dye to track the distribution of liposomes *in vivo*. DiR-LPs distribution *in vivo* was observed in 4T1 breast tumor-bearing BALB/c female mice. As shown in Fig. 10A–B hours post-tail vein injection, the fluorescent signal of DiR-LPs began to arise at the tumor site and reached a peak at 48 h and could last up to 120 h. In addition, tumors and main organs were isolated 48 h post-injection, and the average fluorescence intensity was quantified (Fig. 10C–D). The results revealed that liposome accumulation was much higher in tumors and livers. This passive targeting effect of tumors was primarily attributed to two factors: the modification of polyethylene glycol on the surface of liposomes to enhance liposome permeability and retention, and the EPR effect [32, 33]. The EPR effect increased the accumulation of liposomes with particle sizes of around 100 nm on the interior tissues of the tumor, leading to a targeted effect. PT-54-LPs had both of these characteristics, therefore, it was able to accumulate in the tumor tissue. The accumulation of liposomes

in the liver may be the result of phagocytosis by cells of the reticuloendothelial system (RES) [34]. The reticuloendothelial system is a biological filtration system, that is abundant in the liver and can effectively separate foreign substances from the bloodstream, which leads to the inevitable uptake of some liposomes by the reticuloendothelial system.

In vivo antitumor efficacy

Drugs encapsulated by liposomes could reduce systemic cytotoxicity and target tumor lesions by the EPR effect, prolong drug residence time in the circulation, and enhance antitumor activity [35, 36]. Therefore, although PT-54-LPs did not exhibit better cell inhibitory effects *in vitro* than free PT-54, since *in vitro* and *in vivo* studies, we further investigated the antitumor effects of PT-54-LPs *in vivo*. We established the 4T1 subcutaneous tumor models of BALB/c female mice and designed a therapeutic schedule for *in vivo* tumor inhibition studies (Fig. 11A).

Tumor growth results (Fig. 11B) showed that there was no significant difference in tumor volume between the PBS group and the Blank LPs group, indicating that the Blank LPs have almost no antitumor effect. This result was consistent with the results of *in vitro* cytotoxicity assessment (the survival rate of the tumor cells was over 90% after treatment with different concentrations of blank liposome groups), and the tumor growth rate was slower in the other two groups (free PT-54 and PT-54-LPs) as compared to the control group. More importantly, the tumor inhibitory effect was the most significant in the PT-54-LPs group. On day 13, the mean volume of tumors in the free PT-54 group was $597.63 \pm 61.67 \text{ mm}^3$, which was much larger than that of the PT-54-LPs group (352.02 ± 33.67

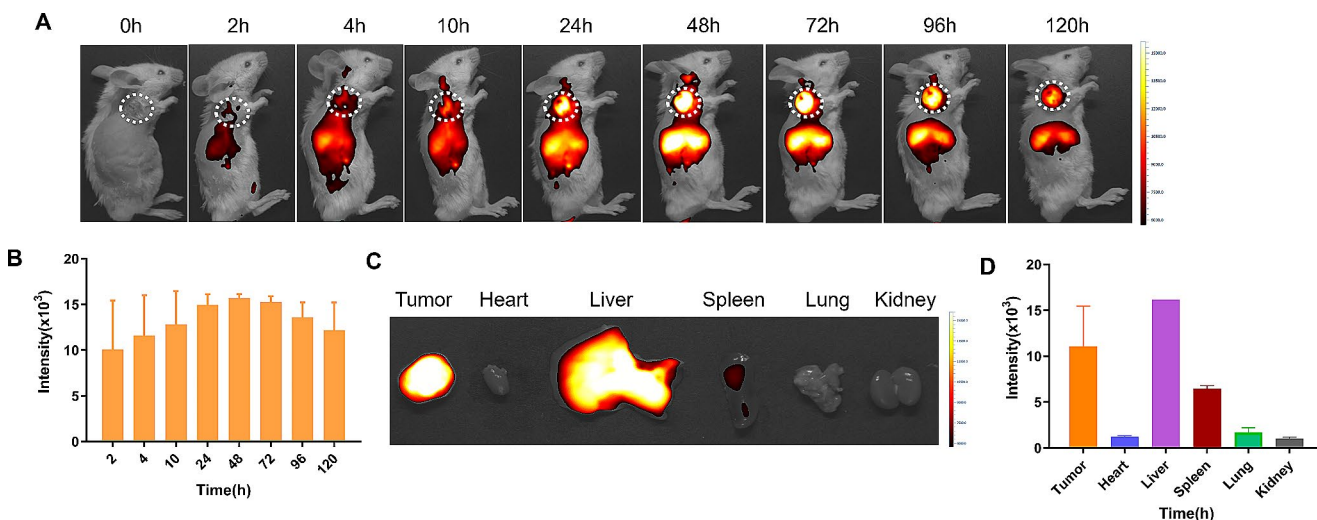


Fig. 10 NIR fluorescence imaging results of DiR-LPs in 4T1 tumor model. (A) Representative *in vivo* NIR fluorescence images of mice after an *i. v.* injection of DiR-LPs. (B) The quantification of the NIR fluorescence signal intensity in tumors at predetermined time points

after *i. v.* injection. (C) The NIR fluorescence images of main organs after 48 h *i. v.* post-injection. (D) The quantification of the NIR fluorescence signal intensity analysis of tumors and major organs after a 48 h *i. v.* post-injection. Data were represented as the mean \pm SD ($n = 3$)

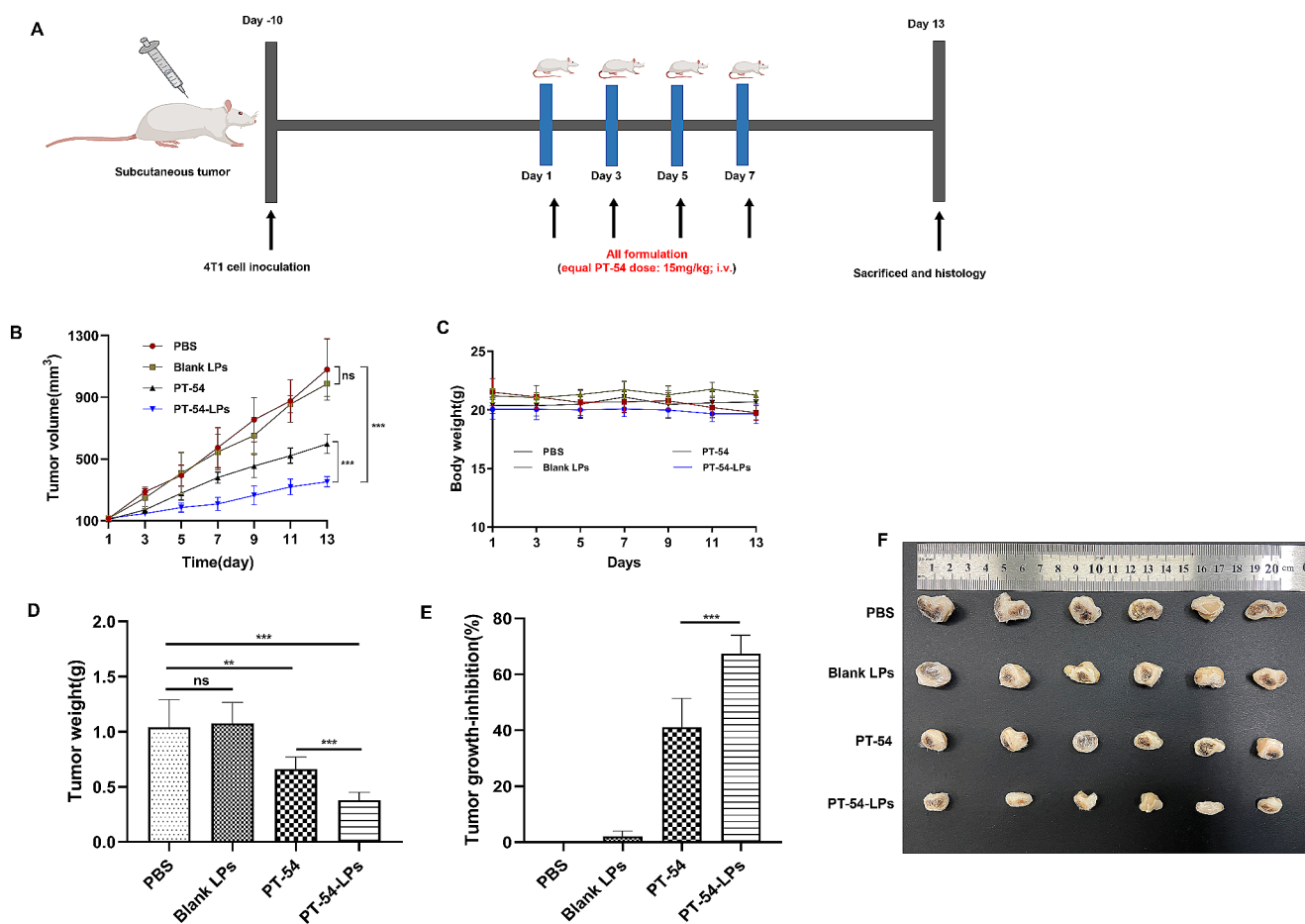


Fig. 11 In vivo anti-tumor efficacy of PT-54-LPs in 4T1 tumor model. (A) The therapeutic schedule of in vivo tumor inhibition study. (B) Tumor volume of mice after different treatments. (C) Body weight changes in mice after various treatments. (D) Tumor weights of mice after different treatments. (E) The tumor growth-inhibition rate was

calculated according to the formula. (F) Photos of representative tumor tissues were obtained on day 13. Data were represented as mean \pm SD ($n \geq 6$), where **: $p < 0.01$, ***: $p < 0.001$, compared with the indicated group

mm³, $p < 0.001$). All mice were executed, and the tumors were collected, weighed, and photographed on day 13. As shown in Fig. 11D, the average tumor weight in the PT-54-LPs-treated group (0.38 ± 0.07 g) was significantly lower than that of the free PT-54 (0.61 ± 0.16 g) ($p < 0.001$) and PBS (1.04 ± 0.25 g) ($p < 0.001$)-treated groups. Meanwhile, tumor inhibition was $67.5 \pm 6.44\%$ in the PT-54-LPs group, which was much higher ($p < 0.001$) than the free PT-54 group ($41.33 \pm 10.33\%$) (Fig. 11E). Tumor images further validated the significant anti-tumor efficacy of PT-54-LPs (Fig. 11F).

H&E staining of the tumor section was further evaluated. As shown in Fig. 12, cancer cells treated with the PBS group and the Blank LPs group showed no substantial necrosis, and their nuclei were preserved in their whole state. On the contrary, tumor cells treated with PT-54 formulations had smaller nuclei and lower cellular density, indicating that tumor cell growth was inhibited. Furthermore, tumors treated with PT-54-LPs exhibited more apoptotic cells, extensive nuclear shrinkage, and necrotic areas than the free PT-54 group. These

results additionally indicated that PT-54-LPs showed more effective anti-tumor ability in vivo than free PT-54. Notably, the anticancer effects of drugs were inconsistent in vitro and in vivo, as free PT-54 exhibited higher cytotoxicity in vitro than PT-54-LPs, however, PT-54-LPs showed better antitumor effects in vivo than free PT-54. It has been reported that free drugs were more cytotoxic compared to nanodrugs in vitro; however, nanodrugs showed better antitumor effects than free drugs in vivo [24, 37]. The reason for this phenomenon might be that free drugs could rapidly enter tumor cells by diffusion, while nanodrugs had obvious slow-release characteristics, therefore, nanodrugs showed lower cytotoxicity to tumor cells in vitro and better anti-tumor activity in vivo compared with free drugs. Most importantly, nanodrugs could prevent drug degradation, prolong drug circulation time in the bloodstream, and enhance antitumor activity by targeting tumors through the EPR effect [36]. Based on the EPR effect, liposomes could effectively target drug delivery to the tumor locations while reducing renal excretion and metabolism, prolonging

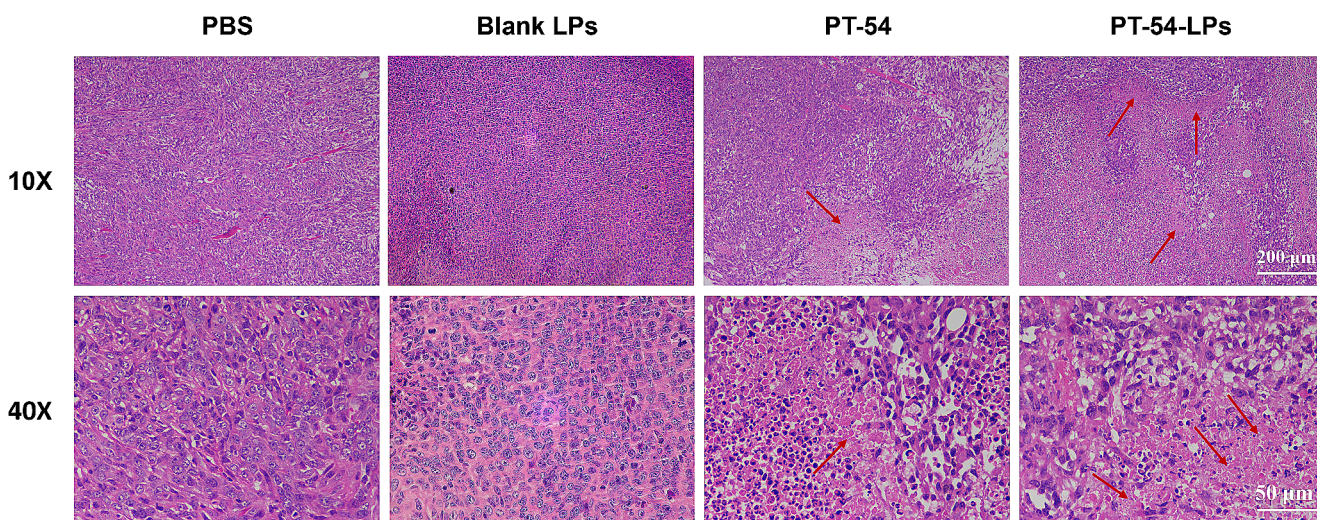


Fig. 12 Representative histological features of 4T1 tumor tissue sections after different treatments

the duration of drug action in the body. Therefore, PT-54-LPs exhibited better antitumor efficacy *in vivo*.

Preliminary safety study of PT-54-LPs

Changes in body weight were monitored from 1 to 13 days to assess the toxicity of PBS, Blank LPs, free PT-54, and PT-54-LPs (Fig. 11C). There was no significant decrease in body weight in Blank LPs and PT-54-LPs groups of mice compared

to the PBS group, but in the free PT-54 group, there was a trend of slow decrease in body weight of mice after administration, which might be related to the toxicity of free PT-54.

To assess the systemic toxicity of Blank LPs, free PT-54, and PT-54-LPs, we evaluated the hematological, liver, and kidney function indexes of mice treated with different PT-54 formulations. As shown in Fig. 13, there were no significant differences in all the indexes in the Blank LPs group and PT-54-LPs group compared with the PBS group, however, the

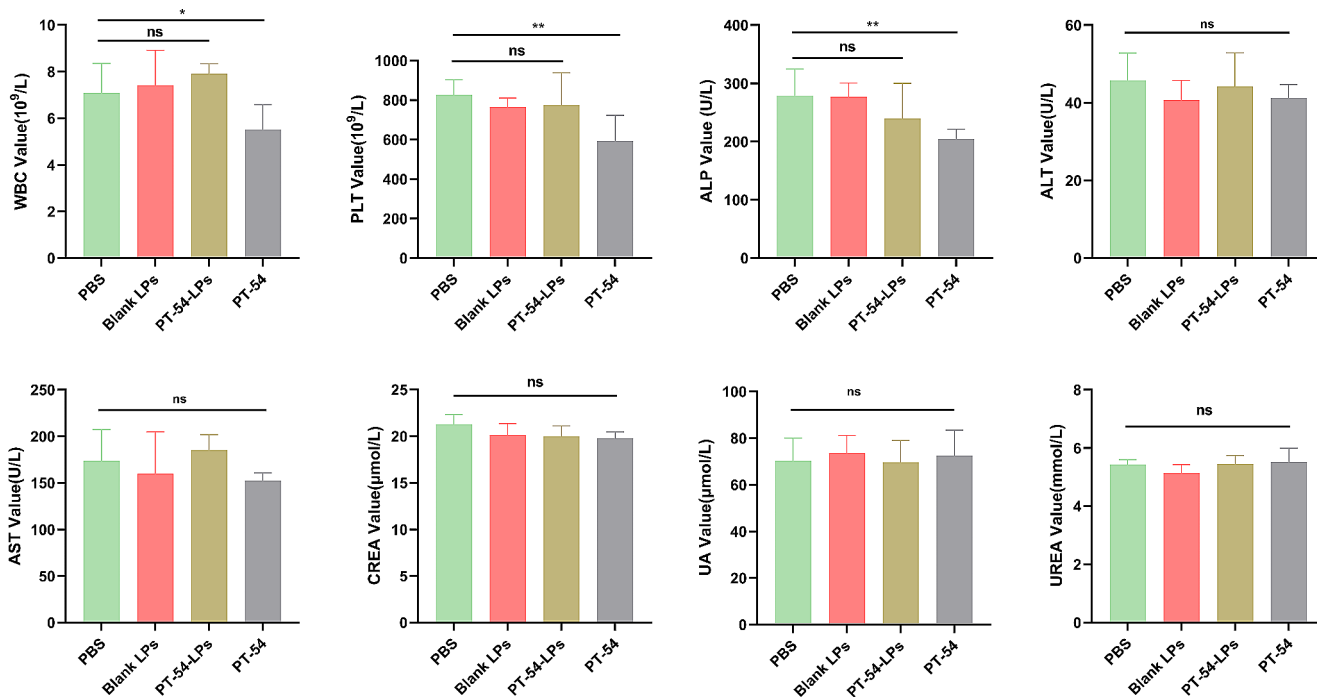


Fig. 13 Evaluation of the systemic toxicity of PT-54-LPs. Hematology analysis (WBC, white blood cells; PLT, platelet). The liver functions (ALP, alkaline phosphatase; ALT, alanine aminotransferase; AST, aspartate aminotransferase) and the renal functions (CREA, creatinine;

UA, uric acid; UREA, urea) were tested. Data were represented as mean ± SD ($n \geq 6$), where ns: $p > 0.05$, *: $p < 0.05$, **: $p < 0.01$, compared with the PBS group

free PT-54 group showed a significantly decreased number of white blood cells ($WBC=5.51 \times 10^9/L$) ($p < 0.05$) and platelets ($PLT=593 \times 10^9/L$) ($p < 0.01$) compared with the PBS group ($WBC=7.07 \times 10^9/L$, $PLT=826 \times 10^9/L$). According to the previous study, decreased white blood cell count was one of the common symptoms following the use of tumor chemotherapy drugs [38], and thrombocytopenia was also a common hematologic disease following the use of HDACs inhibitors [39, 40]. However, PT-54-LPs showed no influence on these indexes. This suggested that free PT-54 might have severe immunosuppressive effects. Alkaline phosphatase was primarily derived from the liver [41], and a low alkaline phosphatase level indicated liver dysfunction. Blood biochemical analysis showed that the free PT-54 group reduced alkaline phosphatase (ALP) levels compared with the PBS group, indicating that free PT-54 induced hepatic injury, however, no significant adverse effects in the PT-54-LPs group were detected. It might

be attributed to the fact that after being encapsulated into the liposomes, PT-54 was effectively targeted and delivered to the tumor microenvironment by the EPR effect, which improved the efficacy of the drug while decreasing its distribution into other non-targeted organs and tissues, therefore reducing its toxicity in vivo.

Furthermore, we evaluated the safety of Blank LPs, free PT-54, and PT-54-LPs in essential organs. Histological analysis of the main organs of mice was used to assess the systemic toxicity of PT-54 drugs. As shown in Fig. 14, there was obvious nuclei aggregation in the liver tissues of the mice treated by the free PT-54 group, implying that inflammatory cells were generated and caused liver damage in the mice, while there was no obvious damage in the PBS, Blank LPs, and PT-54-LPs groups. Lung metastasis was a common symptom of 4T1 tumors in mice [42], and the lung histopathologic results showed that mice treated with PBS, Blank LPs, and

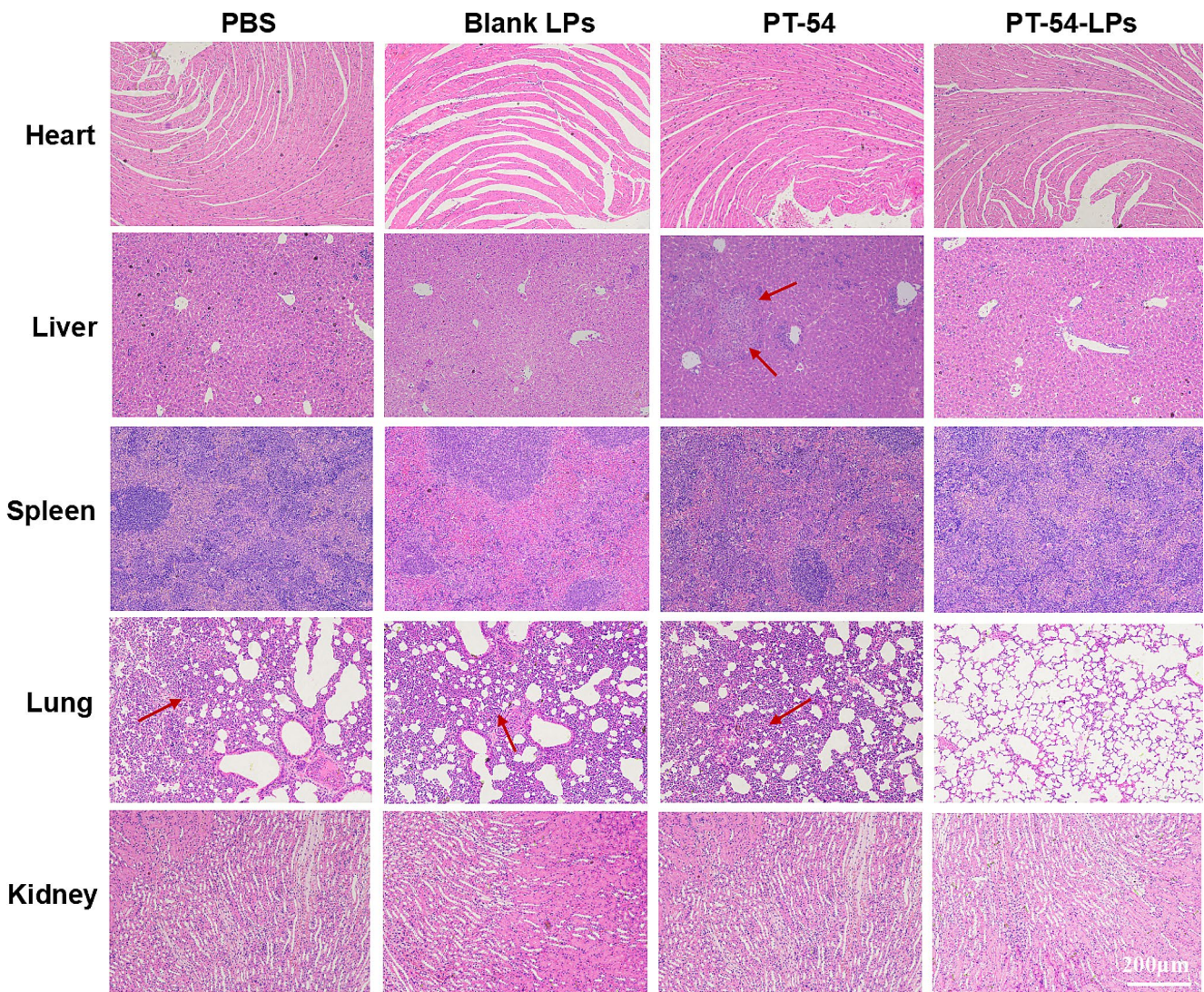


Fig. 14 Results of H & E staining of major organs in mice receiving different treatments. Pictures taken at $100 \times$ magnification

free PT-54 groups developed obvious tumor lung metastasis, while mice treated with PT-54-LPs had no lung metastasis. This indicated that the preparation of PT-54 into liposomes could decrease the toxicity of PT-54 to normal tissues and inhibit tumor lung metastasis simultaneously.

Conclusions

In this study, ALK/HDACs dual target inhibitor liposomes (PT-54-LPs) were prepared by the membrane hydration method, and the liposomes had a regular shape and uniform particle size distribution, with good encapsulation efficiency and serum stability. Most importantly, the defect of poor solubility of PT-54 in water was significantly improved. The PT-54-LPs had an obvious slow-release effect *in vitro*, and the slow-release time was up to 120 h, which ensured the sustained release of the drug *in vivo*, and increased the duration of drug activity. Notably, PT-54-LPs enhanced the drug's anticancer efficacy *in vivo* and reduced the toxicity of PT-54 to the circulatory system and liver. These results indicated that the preparation of PT-54 into liposomes could lead to a higher level of anticancer effects than free PT-54, while significantly reducing the systemic toxicity of PT-54 and providing a promising therapeutic strategy for cancer treatment.

Supplementary Information The online version contains supplementary material available at <https://doi.org/10.1007/s13346-024-01647-1>.

Acknowledgements This work was supported by the Program of Postgraduate Joint Training Base of Chongqing (Chongqing Medical University & Yaopharma Co., Ltd joint training base for postgraduate in pharmacy) (to Huali Chen and Yan Zhang), the Natural Science Foundation of Chongqing Municipal Science and Technology Commission (project no. CSTB2023NSCQ-MSX0086, to Huali Chen), and the Science and Technology Research Program of Chongqing Municipal Education Commission (grant no. KJQN202200451, to Qiangyu Zhang).

Author contributions Fang Ren: Methodology, Investigation, Data curation, Visualization, Writing—original draft. Zongjie Gan: Synthesized API (PT-54), Conceptualization, Investigation, Resources. Qianyu Zhang: Funding acquisition, Methodology, Writing - review & editing. Dan He: Methodology, Investigation, Validation. Baoyan Chen: Established animal tumor models, Formal analysis. Xianwei Wu: Animal anatomical sampling experiment, Visualization. Xiaolin Zeng: Animal anatomical sampling experiment, Data curation. Kexin Wu: Animal experiment fluorescence data analysis, Software. Yangchen Xing: Animal blood collection experiment, Investigation. Yan Zhang: Funding acquisition. Huali Chen*: Funding acquisition, Conceptualization, Supervision, Writing - review & editing. All authors read and approved the final manuscript.

Funding The Program of Postgraduate Joint Training Base of Chongqing (Chongqing Medical University & Yaopharma Co., Ltd joint training base for postgraduate in pharmacy) (to Huali Chen and Yan Zhang). The Natural Science Foundation of Chongqing Municipal Science and

Technology Commission (project no. CSTB2023NSCQ-MSX0086, to Huali Chen).

The Science and Technology Research Program of Chongqing Municipal Education Commission (grant no. KJQN202200451, to Qiangyu Zhang).

Data availability The datasets generated during or analyzed during the current study are available from the corresponding author on reasonable request.

Declarations

Ethics approval This study was conducted following the principles of the Declaration of Helsinki and was approved by the Institutional Review Board of Chongqing Management Approach of Laboratory Animals (Chongqing government order NO.195).

Consent for publication Not applicable.

Competing interests The authors declare that they have no known competing financial interests or personal relationships that could have appeared to influence the work reported in this paper.

References

- 1 Ghosh S, et al. Triple negative breast cancer and non-small cell lung cancer: clinical challenges and nano-formulation approaches. *J Control Release*. 2021;337:27–58.
- 2 Chang E, et al. Porphyrin-lipid stabilized paclitaxel nanoemulsion for combined photodynamic therapy and chemotherapy. *J Nanobiotechnol*. 2021;19(1):154.
- 3 Xian C, et al. Platinum-based chemotherapy via nanocarriers and co-delivery of multiple drugs. *Biomater Sci*. 2021;9(18):6023–36.
- 4 Zhao S, et al. New perspectives for targeting therapy in ALK-positive human cancers. *Oncogene*. 2023;42(24):1959–69.
- 5 Mottet D, Castronovo V. Histone deacetylases: target enzymes for cancer therapy. *Clin Exp Metastasis*. 2008;25(2):183–9.
- 6 Pan T, et al. Discovery of 2,4-pyrimidinediamine derivatives as potent dual inhibitors of ALK and HDAC. *Eur J Med Chem*. 2021;224:113672.
- 7 Patra JK, et al. Nano based drug delivery systems: recent developments and future prospects. *J Nanobiotechnol*. 2018;16(1):71.
- 8 Fang Y, et al. EGFR-targeted multifunctional polymersomal doxorubicin induces selective and potent suppression of orthotopic human liver cancer *in vivo*. *Acta Biomater*. 2017;64:323–33.
- 9 Wuttke S, et al. Positioning metal-organic framework nanoparticles within the context of drug delivery - a comparison with mesoporous silica nanoparticles and dendrimers. *Biomaterials*. 2017;123:172–83.
- 10 Al-Jamal WT, Kostarelos K. Liposomes: from a clinically established drug delivery system to a nanoparticle platform for therapeutic nanomedicine. *Acc Chem Res*. 2011;44(10):1094–104.
- 11 Zuo T, et al. RGD(arg-Gly-Asp) internalized docetaxel-loaded pH sensitive liposomes: Preparation, characterization and antitumor efficacy *in vivo* and *in vitro*. *Colloids Surf B Biointerfaces*. 2016;147:90–9.
- 12 Okamoto Y, et al. Preparation, characterization, and *in vitro/in vivo* evaluation of paclitaxel-bound albumin-encapsulated liposomes for the treatment of pancreatic Cancer. *ACS Omega*. 2019;4(5):8693–700.
- 13 Chen L, et al. Effect of integrin receptor-targeted liposomal paclitaxel for hepatocellular carcinoma targeting and therapy. *Oncol Lett*. 2021;21(5):350.

- 14 Jiang H, et al. Liver-targeted liposomes for codelivery of curcumin and combretastatin A4 phosphate: preparation, characterization, and antitumor effects. *Int J Nanomed.* 2019;14:1789–804.
- 15 Wang M, et al. Pharmacokinetic and pharmacodynamic study of a phospholipid-based phase separation gel for once a month administration of octreotide. *J Control Release.* 2016;230:45–56.
- 16 Yang Z, et al. pH multistage responsive micellar system with charge-switch and PEG layer detachment for co-delivery of paclitaxel and curcumin to synergistically eliminate breast cancer stem cells. *Biomaterials.* 2017;147:53–67.
- 17 Deshantri AK, et al. Nanomedicines for the treatment of hematological malignancies. *J Control Release.* 2018;287:194–215.
- 18 Kuai R, et al. Efficient delivery of payload into tumor cells in a controlled manner by TAT and thiolytic cleavable PEG co-modified liposomes. *Mol Pharm.* 2010;7(5):1816–26.
- 19 Shi Y, et al. The EPR effect and beyond: strategies to improve tumor targeting and cancer nanomedicine treatment efficacy. *Theranostics.* 2020;10(17):7921–4.
- 20 Kalyane D, et al. Employment of enhanced permeability and retention effect (EPR): nanoparticle-based precision tools for targeting of therapeutic and diagnostic agent in cancer. *Mater Sci Eng C Mater Biol Appl.* 2019;98:1252–76.
- 21 Farooq MA, et al. Enhanced cellular uptake and cytotoxicity of vorinostat through encapsulation in TPGS-modified liposomes. *Colloids Surf B Biointerfaces.* 2021;199:111523.
- 22 Srihera N, et al. Preparation and characterization of astaxanthin-loaded liposomes stabilized by Sea Cucumber Sulfated Sterols instead of cholesterol. *J Oleo Sci.* 2022;71(3):401–10.
- 23 Pereira S et al. Lipoplexes to deliver oligonucleotides in Gram-positive and Gram-negative Bacteria: towards treatment of blood infections. *Pharmaceutics.* 2021; 13(7).
- 24 Wang R, et al. Smart pH-responsive polyhydralazine/bortezomib nanoparticles for remodeling tumor microenvironment and enhancing chemotherapy. *Biomaterials.* 2022;288:121737.
- 25 Jiang T, et al. Dual-functional liposomes based on pH-responsive cell-penetrating peptide and hyaluronic acid for tumor-targeted anticancer drug delivery. *Biomaterials.* 2012;33(36):9246–58.
- 26 Assali M, et al. Single-walled carbon nanotubes-ciprofloxacin nanoantibiotic: strategy to improve ciprofloxacin antibacterial activity. *Int J Nanomed.* 2017;12:6647–59.
- 27 Wang S et al. Liposomes for Tumor targeted therapy: a review. *Int J Mol Sci.* 2023; 24(3).
- 28 Chen Y, et al. A lyophilized sterically stabilized liposome-containing docetaxel: in vitro and in vivo evaluation. *J Liposome Res.* 2017;27(1):64–73.
- 29 Liu T, et al. Preparation of Glycyrrhetic Acid liposomes using lyophilization monophasic solution method: Preformulation, optimization, and in Vitro evaluation. *Nanoscale Res Lett.* 2018;13(1):324.
- 30 Yan H, et al. Disulfiram inhibits IL-1 β secretion and inflammatory cells recruitment in aspergillus fumigatus keratitis. *Int Immunopharmacol.* 2022;102:108401.
- 31 Cai M, et al. In vitro and in vivo anti-tumor efficiency comparison of phosphorylcholine micelles with PEG micelles. *Colloids Surf B Biointerfaces.* 2017;157:268–79.
- 32 Kang H, et al. Size-dependent EPR effect of polymeric nanoparticles on Tumor Targeting. *Adv Healthc Mater.* 2020;9(1):e1901223.
- 33 Maruyama K. Intracellular targeting delivery of liposomal drugs to solid tumors based on EPR effects. *Adv Drug Deliv Rev.* 2011;63(3):161–9.
- 34 Zahednezhad F, et al. Liposome and immune system interplay: challenges and potentials. *J Control Release.* 2019;305:194–209.
- 35 Dianat-Moghadam H, et al. Cancer stem cells-emanated therapy resistance: implications for liposomal drug delivery systems. *J Control Release.* 2018;288:62–83.
- 36 Su Z, et al. Novel nanomedicines to overcome cancer multidrug resistance. *Drug Resist Updat.* 2021;58:100777.
- 37 Li T, et al. Efficacy analysis of targeted nanodrug for non-small cell lung cancer therapy. *Front Bioeng Biotechnol.* 2022;10:1068699.
- 38 Chen, Yuxin et al. Reassembling of albumin-bound paclitaxel mitigates myelosuppression and improves its antitumoral efficacy via neutrophil-mediated targeting drug delivery. *Drug Delivery.* 2022.
- 39 Heideman MR, et al. Sin3a-associated Hdac1 and Hdac2 are essential for hematopoietic stem cell homeostasis and contribute differentially to hematopoiesis. *Haematologica.* 2014;99(8):1292–303.
- 40 Wilting Roel H et al. Overlapping functions of Hdac1 and Hdac2 in cell cycle regulation and haematopoiesis. *EMBO J.* 2010.
- 41 Fernandez NJ, Kidney BA. Alkaline phosphatase: beyond the liver. *Vet Clin Pathol.* 2007;36(3):223–33.
- 42 Pereira ER, et al. Lymph node metastases can invade local blood vessels, exit the node, and colonize distant organs in mice. *Science.* 2018;359(6382):1403–7.

Publisher's Note Springer Nature remains neutral with regard to jurisdictional claims in published maps and institutional affiliations.

Springer Nature or its licensor (e.g. a society or other partner) holds exclusive rights to this article under a publishing agreement with the author(s) or other rightsholder(s); author self-archiving of the accepted manuscript version of this article is solely governed by the terms of such publishing agreement and applicable law.